A Journal of the Gesellschaft Deutscher Chemiker

Angewandte International Edition Chemie

www.angewandte.org

2016–55/48

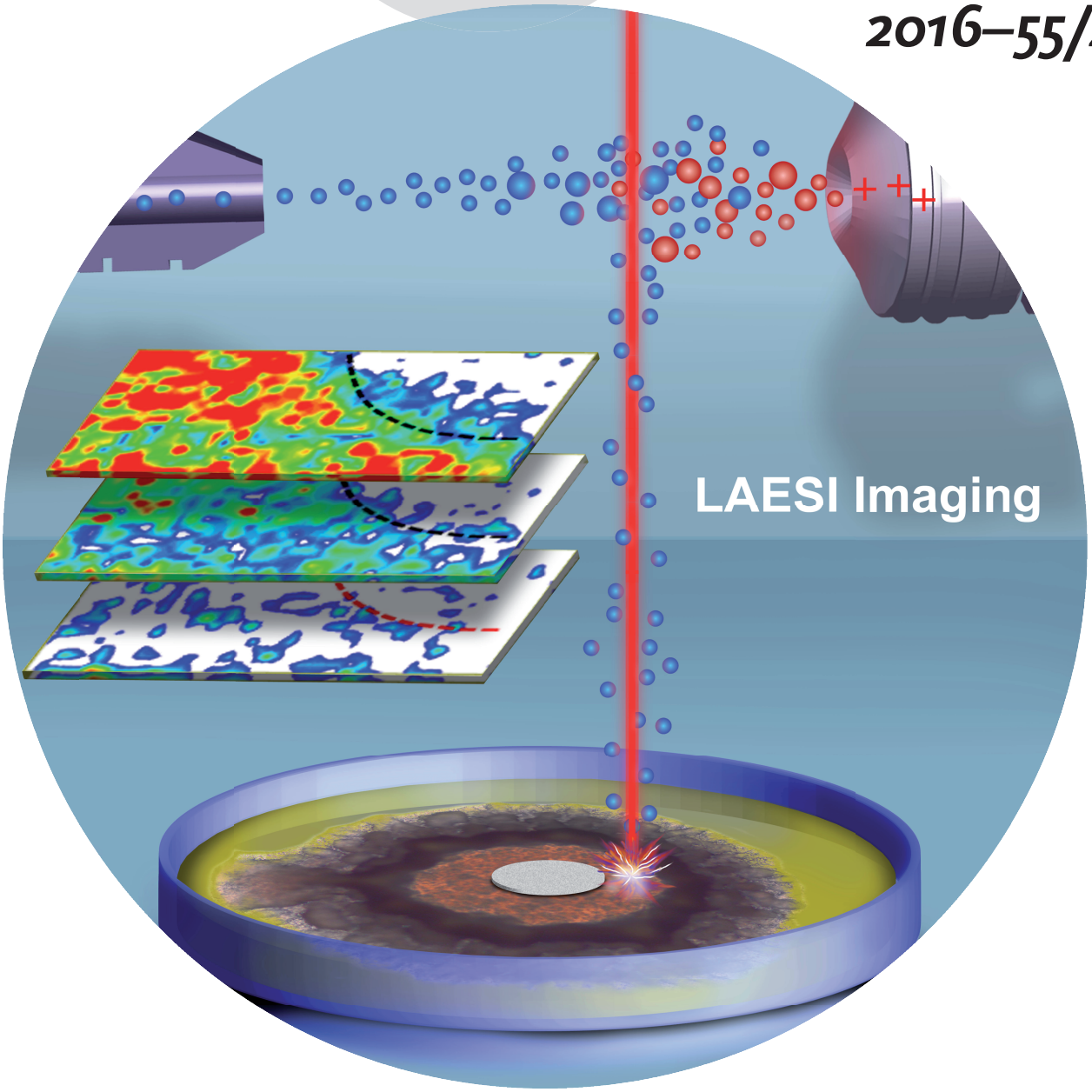

Visualizing the interaction zone

Rapidly emerging microbial resistance to antibiotics is a growing concern for the treatment of infectious diseases. In their Communication on page 15035 ff., A. Vertes et al. describe the application of laser ablation electrospray ionization (LAESI) in combination with mass spectrometry (MS) to gain deeper molecular insight into microbe–antibiotic interactions. LAESI-MS imaging enhances the quantitative nature of antibiotic susceptibility testing, while significantly reducing the required incubation time.

WILEY-VCH

Molecular Imaging Hot Paper

International Edition: DOI: 10.1002/anie.201607751
German Edition: DOI: 10.1002/ange.201607751

Molecular Imaging of Growth, Metabolism, and Antibiotic Inhibition in Bacterial Colonies by Laser Ablation Electrospray Ionization Mass Spectrometry

*Hang Li, Pranav Balan, and Akos Vertes**

Abstract: *Metabolism in microbial colonies responds to competing species, rapidly evolving genetic makeup, and sometimes dramatic environmental changes. Conventional characterization of the existing and emerging microbial strains and their interactions with antimicrobial agents, e.g., the Kirby–Bauer susceptibility test, relies on time consuming methods with limited ability to discern the molecular mechanism and the minimum inhibitory concentration. Assessing the metabolic adaptation of microbial colonies requires their non-targeted molecular imaging in a native environment. Laser ablation electrospray ionization (LAESI) is an ambient ionization technique that in combination with mass spectrometry (MS) enables the analysis and imaging of numerous metabolites and lipids. In this contribution, we report on the application of LAESI-MS imaging to gain deeper molecular insight into microbe–antibiotic interactions, and enhance the quantitative nature of antibiotic susceptibility testing while significantly reducing the required incubation time.*

With the emergence of multidrug resistant microbial strains and bacterial pathogens, the need for rapid and accurate testing of antibiotic susceptibility is increasing.[1–3] Understanding microbial metabolism and its inhibition by the antibiotic is important for developing new treatments of bacterial infections.

Conventional antibiotic susceptibility testing (e.g., the Kirby–Bauer (KB) method) has been widely used for determining drug resistance in clinical microbiology.[4] However, these techniques require a relatively long incubation time of 16–24 h and lack the capability of determining the minimum inhibitory concentration (MIC). Their efficacy is limited for polypeptide antibiotics, anaerobic, slow growing or fastidious bacteria.[5] More recent commercialized versions of the KB approach, e.g., M.I.C.Evaluator and Etest, provide MIC values for different microbial colonies based on test strips with built-in antibiotics gradients.[6]

[*] Dr. H. Li, Prof. A. Vertes
Department of Chemistry, The George Washington University
Washington, DC 20052 (USA)
E-mail: vertes@gwu.edu
Homepage: http://vertes.columbian.gwu.edu
P. Balan
Thomas Jefferson High School for Science and Technology
Alexandria, VA 22312 (USA)
Supporting information and the ORCID identification number(s) for the author(s) of this article can be found under http://dx.doi.org/10.1002/anie.201607751.

Emerging antimicrobial susceptibility testing techniques, including microarrays, whole-genome sequencing, and polymerase chain reaction-based approaches, have all shown promise but it remains to be determined if they possess sufficient sensitivity and specificity.[7,8] Mass spectrometry (MS) was also introduced for studying the resistance of bacteria to various antimicrobial agents. With matrix-assisted laser desorption ionization (MALDI) time-of-flight (TOF) MS, susceptible and resistant isolates of selected microbial model systems, such as *Escherichia coli*, *Staphylococcus aureus*, *Pseudomonas aeruginosa*, were distinguished based on mass spectral features obtained from whole cell pellets or extracts.[8]

In addition, MS and MS imaging (MSI) have played an important role in characterizing the microbial metabolism and investigating the interactions between different phenotypes of bacteria.[9] Secondary ion MS (SIMS)[10] and MALDI-MS,[11,12] as the ionization source under vacuum condition, allowed for high resolution imaging of biomolecular distributions in bacterial communities or interacting microbial colonies. Laser desorption postionization (LDPI) MS with vacuum ultraviolet single photon ionization also enabled the imaging and depth profiling of bacterial biofilms.[13,14] Ambient ionization based MS techniques, such as desorption electrospray ionization (DESI),[15] nano-DESI,[16,17] paper spray,[18] and swab touch spray ionization,[19,20] have been recently developed for imaging and rapid metabolic analysis of microbes in their native environment.

Laser ablation electrospray ionization (LAESI)-MS, an ambient ionization technique, is a tool for the detection, imaging, and depth profiling of metabolites in biological cells and tissues. Both two-dimensional (2D) and three-dimensional (3D) imaging was demonstrated for animal and plant tissues.[21,22] The distribution of a large variety of metabolites and lipids were mapped on tissue sections and meaningful correlations with biological functions were observed. Recently, integrating ion mobility separation (IMS) with LAESI-MS or LAESI-MSI facilitated the separation of isobaric ions based on their drift time (DT) and resulted in enhanced metabolite coverage.[23,24]

In this contribution, LAESI-IMS-MS and LAESI-MSI were utilized to characterize the distributions of a wide array of metabolites and lipids in *E. coli* (ATCC 12435) and *B. subtilis* (ATCC 6051) model microorganisms interacting with antibiotics in Kirby–Bauer type experiments. Antibiotic inhibition of bacterial growth was investigated using 2D and 3D molecular imaging. Experimental methods and mathematical modeling to probe the antibiotic diffusion process are described in the Supporting Information (SI).

Plotting the ion intensities as a function of DT and *m/z* for *B. subtilis* colonies (see Figure S1 in the SI) illustrated the diverse biomolecules detected by LAESI-IMS-MS. Metabolites, lipids, and multiply charged peptides were separated in different regions of the DT vs. *m/z* plot marked by green ovals. Negative (Figure S1a) and positive ion mode (Figure S1b) results complemented each other, enabling the detection of, e.g., nucleoside phosphates and amino acids, respectively. By combining these two modes, over 400 deisotoped spectral features have been detected. To identify the detected ions, accurate *m/z* measurements, tandem MS, collision cross section (CCS) determination, and database searches were jointly employed. To characterize the quality of identification we adopted the four level scheme introduced by the Metabolomics Standards Initiative.[25] Details of the ion identification process and the quality of identification are described in the SI. Based on these results, lists of identified 24 metabolites (Table S1), 40 lipids (Table S2), and 2 peptides were generated for *B. subtilis* and *E. coli*.

Some of the identified molecules belonged to important metabolic pathways, including purine degradation, and the metabolism of pyrimidine, alanine, glutathione, and glycerophospholipids. Comparing the identified ions in the Gram-positive *B. subtilis* and the Gram-negative *E. coli*, a significant overlap was observed in their metabolites and lipids. Certain molecules, for example surfactin, a cyclic lipopeptide, found only in *B. subtilis*, can serve as biomarkers.

To explore the distribution of endogenous metabolites and lipids within a colony, we performed three-dimensional (3D) LAESI-MSI. Figure 1a shows the optical images of a colony, an ablation crater with ca. 150 μm diameter, and the cross sectional view of a colony with an ablation mark. The thickness of an isolated *E. coli* colony was between 80 to 100 μm. With a single laser pulse (0.9 mJ/pulse) producing a ca. 25 μm deep crater, crude depth profiling can be achieved by acquiring individual spectra from three to four consecutive laser pulses. Collecting depth profiles for every probed position on the surface enabled the construction of 3D molecular images. For example, in Figure 1b the 3D distributions of acetylspermidine at *m/z* 188.177, and PE(16:0/17:1) at *m/z* 704.523 exhibited decreasing intensities in deeper layers with the former retaining a stronger signal on the perimeter (see Figure S2a and c in the SI for identification). As a control, a prominent peak from the agar medium at *m/z* 758.409 showed similar intensities and distributions in different layers, indicating consistent signal regardless of depth.

The ability to determine the distributions of metabolites and xenobiotics enables us to investigate the antibiotic susceptibility of bacterial growth using LAESI-MSI in combination with KB type experiments. An inoculated *B. subtilis* culture plate was treated with a penicillin–streptomycin paper disc. After 18 h of incubation, a zone of inhibition (ZOI) with a diameter of 21 mm was observed (Figure 2a).

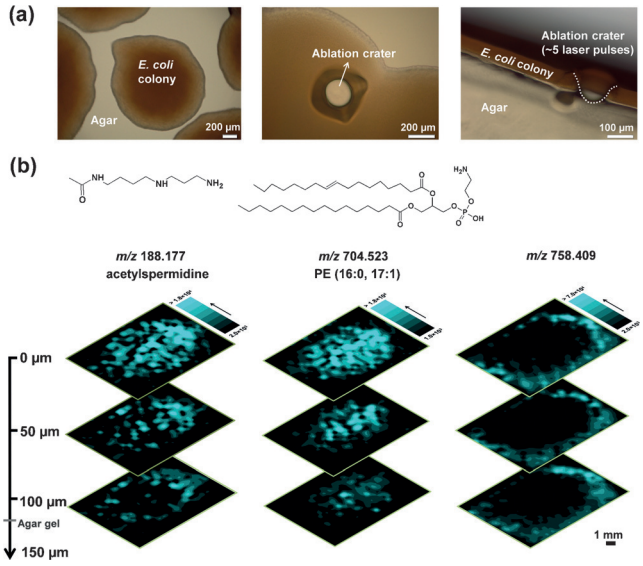

Figure 1. a) Microscope images of *E. coli* colonies. Three images from left to right show a single colony surrounded by neighboring ones, top view of an ablation crater with a diameter of 150 μm, and the side-view indicating the thickness of the colony as 80–100 μm. The side view image also shows the cross sectional view of an ablation crater resulting from five laser pulses. b) Three-dimensional molecular distributions of (left) acetylspermidine at *m/z* 188.177, (middle) PE(16:0/17:1) at *m/z* 704.523, and (right) a prominent peak from the agar medium at *m/z* 758.409.

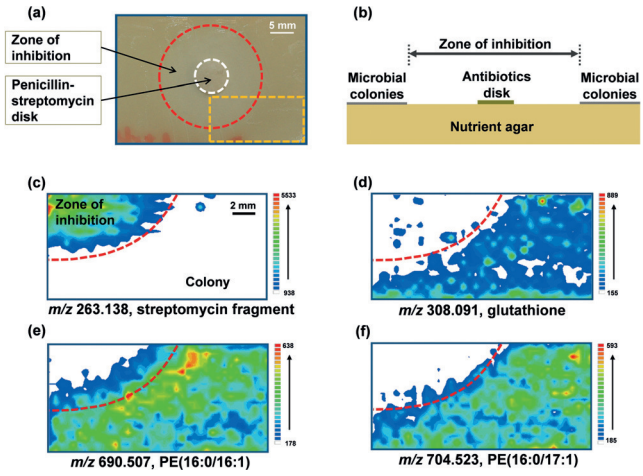

Figure 2. Molecular imaging of antibiotics inhibition on *B. subtilis* colonies. a) *B. subtilis* agar plate after the KB susceptibility testing indicates the produced ZOI (red circle), the penicillin–streptomycin disc (white circle), and the imaged interface region (orange rectangle). b) A side-view schematic of the agar plate reveals the depth dimension, and the antibiotics disc was removed prior to LAESI-MSI. Molecular distribution images of (c) streptomycin fragment at *m/z* 263.138, d) glutathione at *m/z* 308.091, e) PE(16:0/16:1) at *m/z* 690.507, and f) PE(16:0/17:1) at *m/z* 704.523 illustrate the inhibition of *B. subtilis* colonies by the diffusion of streptomycin.

Figure 2b illustrates the cross sectional view showing the antibiotic infused paper disc and the bacterial colonies on top of the agar. The disc was removed prior to the imaging experiment and part of the interface between the ZOI and the colony was imaged (see orange rectangle in Figure 2a). As shown in Figure 2c, the abundance of streptomycin fragment with *m/z* 263.138 was high at the location where the disc has been placed then it decreased towards the edge of the ZOI,

and eventually it was obscured by the bacterial colony. In contrast in Figure 2 d, e and f, the glutathione at *m/z* 308.091 (see Figure S2b in the SI for identification) and the two phosphatidylethanolamine (PE) ions at *m/z* 690.507 and 704.523, respectively, were abundant in the colony but absent in the ZOI. Interestingly, the PE(16:0/16:1) lipid showed increased levels toward the edge of the colony and it was even present in part of the ZOI, whereas, glutathione and PE(16:0/17:1) were not present in the ZOI.

The constructed 3D images (Figure 3) showed the distribution of molecules at three layers of increasing depths of 50 μm each. As the thickness of the colony is ca. 100 μm, the ions detected at depths between 100 and 150 μm included signal from the underlying agar medium. The images of a streptomycin fragment distribution in Figure 3 a reflected both radial and depthwise diffusion away from the disc.

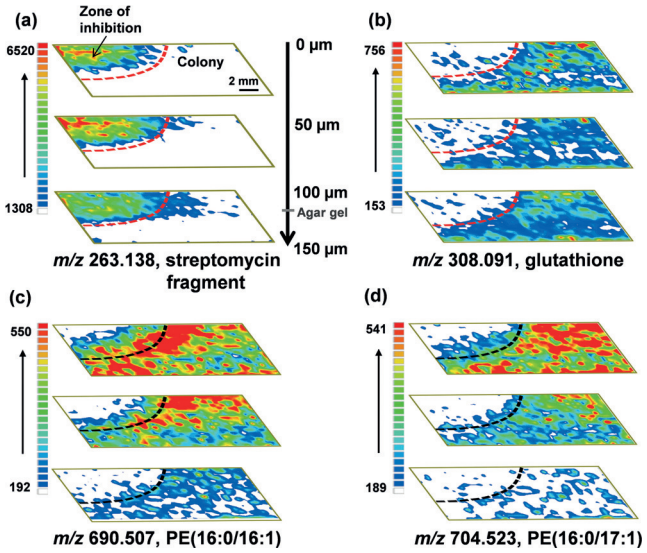

Figure 3. Three-dimensional distributions of a) streptomycin fragment at *m/z* 263.138, b) glutathione at *m/z* 308.091, c) PE(16:0/16:1) at *m/z* 690.507, and d) PE(16:0/17:1) at *m/z* 704.523 in KB susceptibility testing for *B. subtilis*. Streptomycin diffuses both radially and depthwise into the agar. Glutathione exhibits similar distributions in the three layers of increasing depths, whereas lipids PE(16:0/16:1) and PE(16:0/17:1) show a significantly lower abundance in the bottom layer.

Interestingly, streptomycin fragment was detected in the deepest layer even under the colonies, indicating that in these regions the levels of the antibiotic in the agar were below the MIC. Glutathione exhibited distributions that were similar at different depths with slightly higher abundances in the top layer, whereas PE(16:0/17:1) and PE(16:0/16:1) both exhibited a significantly weaker signal from the bottom layer. A possible explanation of relatively high glutathione intensities from the bottom layer was the leakage of this compound from the bacteria followed by diffusion into the top layers of the agar.

Recent investigations of its impact on the susceptibility of some bacteria (*E. coli*) toward streptomycin revealed that glutathione reduced the effectiveness of the antibiotic.[26] Imaging the distribution of glutathione produced by bacteria (*B. subtilis*) in the presence of streptomycin by LAESI-MSI enabled us to determine if the presence of the antibiotic induced elevated levels of glutathione. Observing the related distribution in Figure 3 b, there seems to be no increase in the glutathione intensities close to the zone of inhibition where the streptomycin concentrations are higher.

As different species of bacteria can coexist in an environment, it is interesting to explore their differential inhibition by antibiotics. Two halves of an agar plate were inoculated with *B. subtilis* and *E. coli*, respectively (see inset in Figure 4), and a streptomycin fragment was placed in the center. After 21 h of incubation, molecular distributions of different lipids exhibited distinct features. For example, PE(16:0/17:1) (in protonated and sodiated form), and PE(16:0/18:1) showed significantly higher abundances for the regions inhabited by *B. subtilis* colonies (see Figure 4 a–c), whereas PE(31:1), PE(18:1/18:1), and PG(34:1) were more prevalent in the areas covered by *E. coli* (see Figure 4 d–f). These findings indicate which lipids can be utilized to distinguish between the *B. subtilis* and *E. coli* colonies. To verify that the two optical zone diameters (ZDs) measured in the system with the adjacent colonies of *E. coli* and *B. subtilis* reflect their individual ZDs, we performed the KB susceptibility test on two plates with *E. coli* and *B. subtilis* separately. The observed ZDs for *E. coli* and *B. subtilis* on the single species plates (see

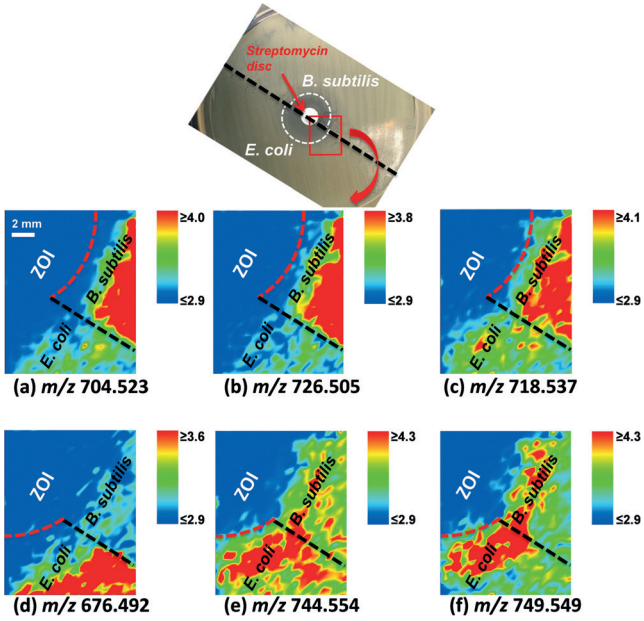

Figure 4. Molecular imaging of antibiotics inhibition on adjacent bacterial colonies separated by black dashed line. The inset shows an agar plate with the top half inoculated with *B. subtilis* and the bottom half with *E. coli*. An antibiotics susceptibility test was performed on the plate with 40 μg streptomycin disc placed in the center. The highlighted red rectangular region corresponds to the imaged area, and molecular distribution images of a) PE(16:0/17:1), $[M+H]^+$, b) PE(16:0/17:1), $[M+Na]^+$, c) PE(16:0/18:1), $[M+H]^+$, d) PE(31:1), $[M+H]^+$, e) PE(18:1/18:1), $[M+H]^+$, and f) PG(34:1), $[M+H]^+$ are displayed. Boundary of ZOI is shown by red dashed line. The label of the false color scale bar is the logarithm of the ion intensity.

Figure S8a and c) were the same as the values determined on the single plate that contained the two colonies adjacent to each other (see Figure S8b in the SI).

Using density profiles derived from optical imaging, a difference was observed between the ZOIs with diameter values of 15.6 mm and 18.0 mm for *B. subtilis* and *E. coli*, respectively. The spatial distributions for the ion with nominaL m/z 719 and 750, reporting on *B. subtilis* and *E. coli*, respectively, determined by LAESI-MSI (see panels c and f in Figure 4) indicated zone diameter (ZD) values of $ZD_{719} = 14.5$ mm and $ZD_{750} = 17.8$ mm, respectively. These results are in good agreement with the optically observed values and indicate reduced susceptibility to streptomycin for *B. subtilis* compared to *E. coli*.

In contrast to ZD_{719} for *B. subtilis* and ZD_{750} for *E. coli* that were close to the optically observed ZD values, the distributions for PE(16:0/17:1) and PE(31:1) in these cultures (see Figure 4a and d) indicated that the ZD_{705} and ZD_{676} for those two lipids were significantly larger than the optically determined ZDs. The dissimilar ZD values for different lipids for a given microorganism indicated that certain biochemical pathways were more efficiently inhibited by the antibiotic. This new insight is provided by the combination of LAESI-MSI and the KB test.

The diffusion of antibiotics in agar was examined using a one-dimensional mathematical model and compared with the experimental data from LAESI-MS. Based on the profiling data for *E. coli* colonies at 21 h (75600 s) of incubation, the detected streptomycin ion intensity profile was fitted using the one-dimensional diffusion model (see Figure S5), whereas the ion abundance profile of PG(34:1) from *E. coli* was fitted using a Gaussian curve to reflect a maximum close to the zone of inhibition. The diffusion coefficient of streptomycin in the agar at 37 °C, $D = 1.3 \times 10^{-6}\ cm^2 s^{-1}$, was determined by fitting the diffusion model to the experimental streptomycin profile. As the intensity of streptomycin signal decreased at the edge of the ZOI, the PG(34:1) signal increased, indicating the growing population of bacteria. The critical concentration (c_{cr}) corresponding to the MIC of streptomycin for *E. coli* was determined as the antibiotic concentration at the position with 50% of the microorganisms inhibited, corresponding to $ZD_{750} = 17.8$ mm in Figure S5. The distribution of this ion closely mirrored the optical density profile of the bacterial colonies. At 21 h of incubation, the streptomycin concentration under the center of the disk was estimated to be 1341 $\mu g\,mL^{-1}$ according to the one-dimensional model described in the SI. The c_{cr} for *E. coli* was determined by comparing the streptomycin concentrations at $x = 8.9$ mm with that at the origin ($x = 0$). The c_{cr} of streptomycin determined for *E. coli* was 240 $\mu g\,mL^{-1}$, which fell in the MIC range reported by the European Committee on Antimicrobial Susceptibility Testing (EUCAST) (the database at http://mic.eucast.org/Eucast2/ was last accessed on January 28, 2016). Alternatively, the c_{cr} of streptomycin for *E. coli* can be calculated based on the Vesterdal model.[27,28] Based on Figure S6 in the SI, a value of 180 $\mu g\,mL^{-1}$ was obtained, which was consistent with our result above. To explore the potential of LAESI-MS for faster assessment of antibiotic susceptibility, we profiled the ion abundance distributions of streptomycin and PE(16:0/16:1) from *E. coli* after 5 h of incubation, a considerably shorter period than the typical 16 to 24 h required for the conventional KB test. The generated results are shown in Figure S9 in the SI. Applying the one-dimensional diffusion model and a sigmoidal growth curve (double Boltzmann) to the streptomycin and PE(16:0/16:1) distributions, respectively, the MIC value was estimated to be 285 $\mu g\,mL^{-1}$ (see Figure S9). This result was consistent with the MIC value obtained at 21 h incubation time (240 $\mu g\,mL^{-1}$), and with the database values.

In conclusion, 2D and 3D molecular imaging by LAESI-MSI of microbial cultures and the inhibition of their growth by antibiotics enriched the concept of the ZOI by distinguishing between the optically detected and molecular distributions. The revealed chemical information has the potential to enhance antibiotic susceptibility testing. A method combining mathematical modeling with LAESI-MS profiling was demonstrated for determining the MIC value after a significantly shorter incubation period. Further, these results indicate the potential of LAESI-MSI to study antibiotic diffusion patterns in tissues qualitatively and quantitatively, and to explore complex bacterial interactions.

Acknowledgements

This material is based upon work supported by the U.S. Department of Energy, Office of Science, Office of Basic Energy Sciences, Chemical Sciences, Geosciences and Biosciences Division under Award Number DE-FG02-01ER15129.

Keywords: antibiotic susceptibility · bacteria · laser ablation electrospray ionization · mass spectrometry · molecular imaging

How to cite: *Angew. Chem. Int. Ed.* **2016**, *55*, 15035–15039
Angew. Chem. **2016**, *128*, 15259–15263

[1] M. A. Fischbach, C. T. Walsh, *Science* **2009**, *325*, 1089–1093.
[2] S. E. Dorman, R. E. Chaisson, *Nat. Med.* **2007**, *13*, 295–298.
[3] T. J. Welch, W. F. Fricke, P. F. McDermott, D. G. White, M.-L. Rosso, D. A. Rasko, M. K. Mammel, M. Eppinger, M. J. Rosovitz, D. Wagner, L. Rahalison, J. E. LeClerc, J. M. Hinshaw, L. E. Lindler, T. A. Cebula, E. Carniel, J. Ravel, *Plos One* **2007**, *2*, e309.
[4] J. H. Jorgensen, M. J. Ferraro, *Clin. Infect. Dis.* **2009**, *49*, 1749–1755.
[5] M. K. Cowan, P. K. Talaro, *Microbiology: A Systems Approach*, McGraw-Hill Higher Education, **2009**.
[6] S. Mushtaq, M. Warner, J. Cloke, M. Afzal-Shah, D. M. Livermore, *J. Antimicrob. Chemother.* **2010**, *65*, 1702–1711.
[7] A. Vertes, V. Hitchins, K. S. Phillips, *Anal. Chem.* **2012**, *84*, 3858–3866.
[8] M. R. Pulido, M. Garcia-Quintanilla, R. Martin-Pena, J. M. Cisneros, M. J. McConnell, *J. Antimicrob. Chemother.* **2013**, *68*, 2710–2717.
[9] J. D. Watrous, P. C. Dorrestein, *Nat. Rev. Microbiol.* **2011**, *9*, 683–694.
[10] D. Debois, K. Hamze, V. Guerineau, J.-P. Le Caer, I. B. Holland, P. Lopes, J. Ouazzani, S. J. Seror, A. Brunelle, O. Laprevote, *Proteomics* **2008**, *8*, 3682–3691.

[11] Y.-L. Yang, Y. Xu, R. D. Kersten, W.-T. Liu, M. J. Meehan, B. S. Moore, N. Bandeira, P. C. Dorrestein, *Angew. Chem. Int. Ed.* **2011**, *50*, 5839 – 5842; *Angew. Chem.* **2011**, *123*, 5961 – 5964.
[12] J. Y. Yang, V. V. Phelan, R. Simkovsky, J. D. Watrous, R. M. Trial, T. C. Fleming, R. Wenter, B. S. Moore, S. S. Golden, K. Pogliano, P. C. Dorrestein, *J. Bacteriol.* **2012**, *194*, 6023 – 6028.
[13] A. Akhmetov, J. F. Moore, G. L. Gasper, P. J. Koin, L. Hanley, *J. Mass Spectrom.* **2010**, *45*, 137 – 145.
[14] C. Bhardwaj, J. F. Moore, Y. Cui, G. L. Gasper, H. C. Bernstein, R. P. Carlson, L. Hanley, *Anal. Bioanal. Chem.* **2013**, *405*, 6969 – 6977.
[15] C. F. F. Angolini, P. H. Vendramini, F. D. S. Araújo, W. L. Araújo, R. Augusti, M. N. Eberlin, L. G. de Oliveira, *Anal. Chem.* **2015**, *87*, 6925 – 6930.
[16] J. Watrous, P. Roach, B. Heath, T. Alexandrov, J. Laskin, P. C. Dorrestein, *Anal. Chem.* **2013**, *85*, 10385 – 10391.
[17] J. Watrous, P. Roach, T. Alexandrov, B. S. Heath, J. Y. Yang, R. D. Kersten, M. van der Voort, K. Pogliano, H. Gross, J. M. Raaijmakers, B. S. Moore, J. Laskin, N. Bandeira, P. C. Dorrestein, *Proc. Natl. Acad. Sci. USA* **2012**, *109*, E1743 – E1752.
[18] A. M. Hamid, A. K. Jarmusch, V. Pirro, D. H. Pincus, B. G. Clay, G. Gervasi, R. G. Cooks, *Anal. Chem.* **2014**, *86*, 7500 – 7507.
[19] A. K. Jarmusch, V. Pirro, K. S. Kerian, R. G. Cooks, *Analyst* **2014**, *139*, 4785 – 4789.
[20] V. Pirro, A. K. Jarmusch, M. Vincenti, R. G. Cooks, *Anal. Chim. Acta* **2015**, *861*, 47 – 54.
[21] P. Nemes, A. A. Barton, A. Vertes, *Anal. Chem.* **2009**, *81*, 6668 – 6675.
[22] P. Nemes, A. S. Woods, A. Vertes, *Anal. Chem.* **2010**, *82*, 982 – 988.
[23] B. Shrestha, A. Vertes, *Anal. Chem.* **2014**, *86*, 4308 – 4315.
[24] H. Li, B. K. Smith, L. Márk, P. Nemes, J. Nazarian, A. Vertes, *Int. J. Mass Spectrom.* **2015**, *377*, 681 – 689.
[25] L. W. Sumner, A. Amberg, D. Barrett, M. H. Beale, R. Beger, C. A. Daykin, T. W. M. Fan, O. Fiehn, R. Goodacre, J. L. Griffin, T. Hankemeier, N. Hardy, J. Harnly, R. Higashi, J. Kopka, A. N. Lane, J. C. Lindon, P. Marriott, A. W. Nicholls, M. D. Reily, J. J. Thaden, M. R. Viant, *Metabolomics* **2007**, *3*, 211 – 221.
[26] M. Goswami, S. H. Mangoli, N. Jawali, *Antimicrob. Agents Chemother.* **2007**, *51*, 1119 – 1122.
[27] D. A. Mitchison, C. C. Spicer, *J. Gen. Microbiol.* **1949**, *3*, 184 – 203.
[28] J. W. Mellor, *Higher Mathematics for Students of Chemistry and Physics*, Longmans, Green and co., London, **1902**.

Received: August 10, 2016
Published online: October 4, 2016

Angewandte
Eine Zeitschrift der Gesellschaft Deutscher Chemiker
Chemie

Supporting Information

Molecular Imaging of Growth, Metabolism, and Antibiotic Inhibition in Bacterial Colonies by Laser Ablation Electrospray Ionization Mass Spectrometry

*Hang Li, Pranav Balan, and Akos Vertes**

anie_201607751_sm_miscellaneous_information.pdf

Supporting Information

Table of Contents

S1. Experimental section

Materials and samples. HPLC grade methanol (A452-4), water (W6-1), chloroform (C607-4), and glacial acetic acid (A35-500) were purchased from Fisher Scientific (Pittsburgh, PA). Poly-DL-alanine (P9003) for CCS calibration was obtained from Sigma-Aldrich (St. Louis, MO).

A starter culture of the lambda derivative of *Escherichia coli* (ATCC 12435, ATCC, Manassas, VA) was grown in a Luria Broth (LB) medium (10855-001, Life Technologies, Frederick, MD) in an orbital shaker (MaxQ 4000, Thermo Scientific Inc., Waltham, MA) at 37 ºC, at 220 rpm. After 24 h of incubation, the liquid culture was inoculated on an LB agar plate (L5542, Sigma-Aldrich, St. Louis, MO) to initiate the colonies for MS study.

For antibiotics susceptibility testing by the Kirby-Bauer (KB) method, a Mueller Hinton (MH) agar plate (R01620, Thermo Scientific, Waltham, MA) was inoculated by liquid cultures of *E. coli* and *Bacillus subtilis* (ATCC 6051, ATCC, Manassas, VA) using a sterile cotton tipped applicator (25-826 5WC, Puritan Medical Products, Guilford, ME). For the experiments presented in Figure 2 and 3, 40.0 µL of the penicillin-streptomycin solution (15070-063, Life Technologies, Carlsbad, CA) was deposited on an antibiotic filter disc (7 mm in diameter). For Figure 4 and Figure S5, 14.8 µL of the streptomycin solution (2700 µg/mL) made from streptomycin sulfate salt (S9137, Sigma-Aldrich, St. Louis, MO) was deposited on a filter disc (6 mm in diameter). The discs were placed onto inoculated plates.

LAESI-IMS-MS and chemical imaging. Microsampling of the bacterial colonies and the agar gel by LAESI utilized mid-IR laser pulses at 2940 nm to induce ablation by sudden energy deposition into the water content of the samples. The ejected ablation plume was intercepted by an electrospray for ionization. To generate the electrospray, the spray solution was delivered at 500 nL/min flow rate through an emitter held at 3300 V voltage. A methanol

chloroform electrospray solution (*v/v* 2:1) with 0.1% acetic acid (*v/v*) was used for both positive and negative ion mode MS. The LAESI-generated ions entered a high performance quadrupole time-of-flight mass spectrometer (Synapt G2S, Waters Co., Milford, MA) through a traveling wave (T-wave) ion mobility separation (IMS) module that measured the collision cross section (CCS) of the ions.

Imaging of the antibiotic, bacterial metabolite and lipid distributions was performed using a commercial LAESI source (DP-1000, Protea Biosciences, Morgantown, WV) integrated with the mass spectrometer. Alternatively, a homebuilt LAESI imaging platform[1] was utilized.

Identification of detected ions. For tandem MS, collision-induced dissociation was performed on selected precursor ions (e.g., *m/z* 188.174, 306.075, 702.507 and 747.523) using collision energies between 15 and 35 eV. Comparing the measured tandem mass spectra with fragmentation database information or fragmentation pattern of reference standards analyzed under identical conditions revealed the molecular structures, e.g., for acetylspermidine and glutathione (see Figure S2a and b). For lipids, for example, a phosphatidylethanolamine, PE(16:0/17:1), and a phosphatidylglycerol, PG(16:0/18:1), the lengths of the acyl chains were determined from the tandem mass spectra (see Figure S2c and d).

Measured CCS values provided additional information to assist in ion identification. Among the major membrane lipids, a large variety of PEs and PGs with different degrees of saturation were distinguished in the mass spectra. By plotting the CCS values for each subclass of lipids as a function of the combined acyl chain lengths, linear trends were observed for lipids with the same degree of saturation (see Figure S3). For example, the CCS values of the deprotonated PE(n:1) species follows a linear trend as a function of n (see Figure S3a). Thus, the identification of lipid ions, e.g., PE(35:1), can be enhanced by evaluating if its CCS value falls

on the PE(n:1) trend line. Also, for isobaric species with different CCSs, e.g., structural isomers, IMS separation can facilitate identification.

To characterize the quality of identification we adopted the four level scheme introduced by the Metabolomics Standards Initiative.[2] From the over 400 deisotoped spectral features that were detected, 3 compounds were identified at level 1 (identified compounds). They were identified by their accurate masses and by the comparison of both the measured tandem mass spectra and CCS values with those of reference standards analyzed under identical conditions (see Tables S1 and S2). Another 10 compounds were identified at level 2 (putatively annotated compounds). They were identified based on their accurate masses and the comparison of the measured tandem mass spectra to databases. The remaining 53 compounds in Tables S1 and S2, are identified at level 3 (putatively characterized compound classes) include metabolites, fatty acids, and lipids (see Tables S1 and S2).

There are over 330 deisotoped spectral features without assignments. In the classification described above, this corresponds to level 4 (unknown compounds). Although not identified, these compounds are reproducibly detected and can be used in, e.g., mass fingerprinting applications.

Data processing. The collected raw data were processed in MassLynx V4.1 (SCN851, Waters Co. Milford, MA). All the mass spectra were averaged and smoothed using a Savitzky Golay filtering. The DT vs. *m/z* map was visualized through the DriftScope V2.4 (Waters Co. Miford, MA). ProteaPlot (V2.0.1.4, Protea Biosciences, Morgantown, WV) and a scientific visualization package (Origin 9.1, OriginLab Northampton, MA) were utilized to construct the spatial distributions of the selected ions. The collected MS and MSI data have been deposited to the Metabolomics Workbench (http://www.metabolomicsworkbench.org/). The mwTab

FileName is Amygwu_20160809_160650, and DATATRACK_ID is 698. The tentative assignments of the detected ions were performed by searching the ECMDB (http://www.ecmdb.ca/, last accessed on January 28, 2016), METLIN (https://metlin.scripps.edu/, last accessed on August 5, 2016), LIPID MAPS (http://www.lipidmaps.org/, last accessed on August 5, 2016), and HMDB (http://www.hmdb.ca/, last accessed on January 28, 2016) databases. The CCS values for the ions were derived from a calibration process using polyalanine standards and calculated in the DriftScope V2.4 software. The density profile for optical imaging was analyzed using ImageJ (an open-source platform for biological image analysis),[3] and fitted using sigmoid growth function in Origin 9.1.

Mathematical modeling. The diffusion of antibiotics through agar gel was modeled to provide more information on antibiotic-microbial interactions. Fick's laws were implemented with appropriate boundary conditions and a one-dimensional model was derived and visualized using Wolfram Mathematica 9 (Wolfram, Champaign, IL, USA) software. The one-dimensional solution is described as $c(x,t) = \frac{c_0}{2}\left[\mathrm{erf}\left(\frac{a+x}{2\sqrt{D\times t}}\right) - \mathrm{erf}\left(\frac{-a+x}{2\sqrt{D\times t}}\right)\right]$, in which c is the measured concentration, c_0 is the initial concentration, a is the radius of the antibiotic disc, t is the diffusion time, and D is the diffusion coefficient.[4] Figure S4a shows the general behavior of the model through the dimensions of position, time, and concentration. In Figure S4b, the diameter of the zone of inhibition is represented as a function of time. Fitting of this function to data collected from LAESI-MS was implemented through the Origin 9.1 scientific visualization package.

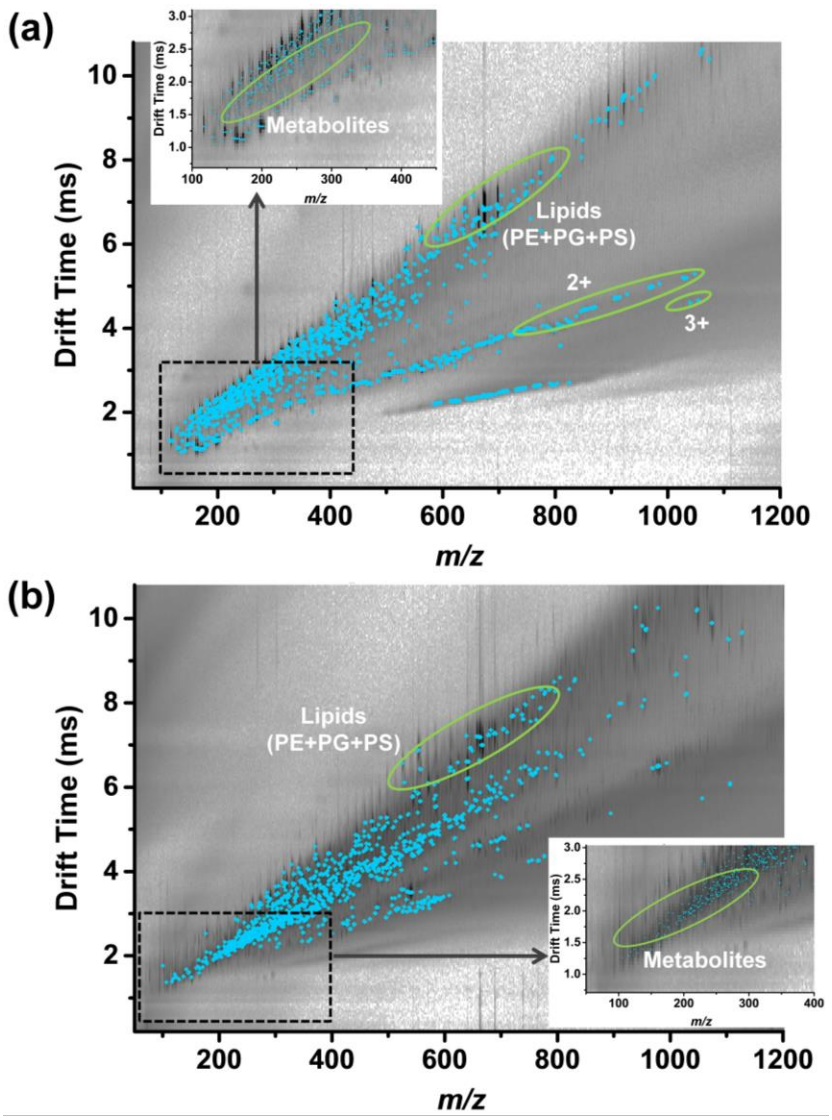

Figure S1. DT vs. m/z maps for ions generated from B. subtilis colonies by LAESI-IMS-MS. (a) In negative ion mode, the green ellipse highlights the regions for detected metabolites, lipids, and doubly and triply charged ions. (b) In positive ion mode, the green ellipse highlights the regions for metabolites and lipid.

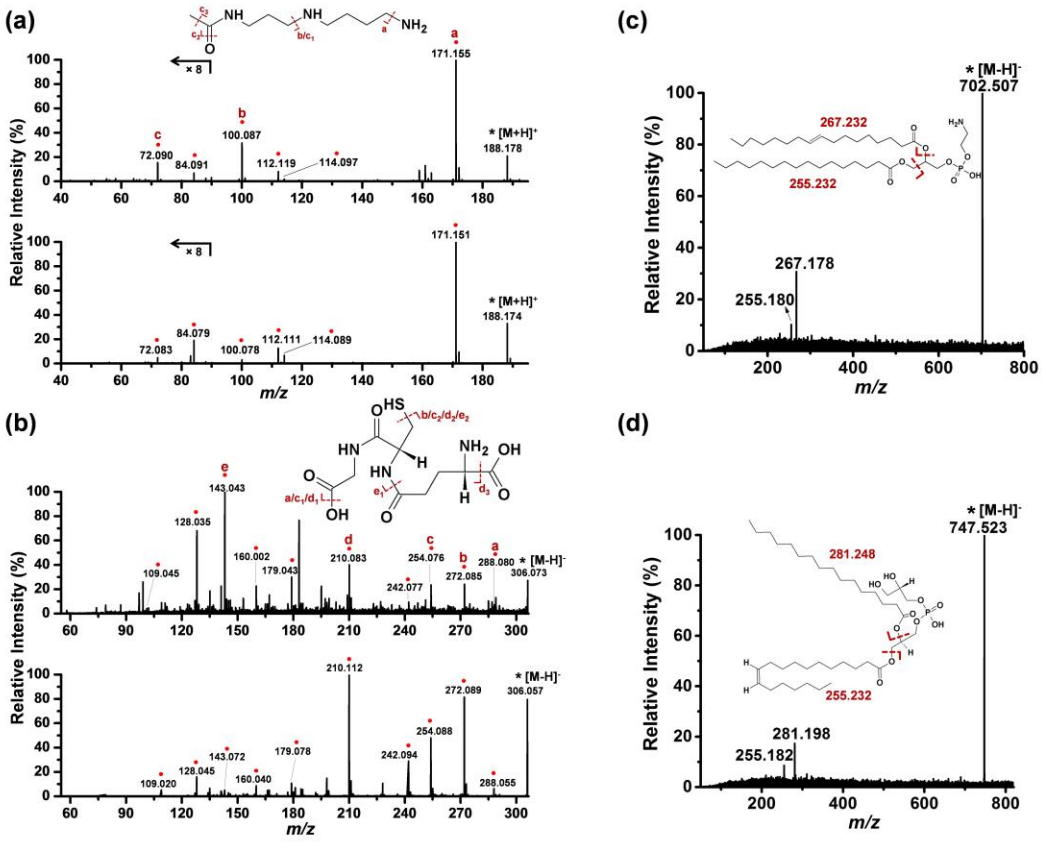

Figure S2. Tandem mass spectra for (a) ion with nominal *m/z* 188 form the acetylspermidine reference standard (top panel) and *B. subtilis* cell pellets (bottom panel), (b) ion with nominal *m/z* 306, from the glutathione reference standard (top panel) and *B. subtilis* cell pellets (bottom panel), (c) ion with *m/z* 702.507 identified as PE(16:0/17:1) from *E. coli* cell pellets, and (d) ion with *m/z* 747.523 identified as PG(16:0/18:1) from *E. coli* cell pellets. Symbol * indicates the parent ions.

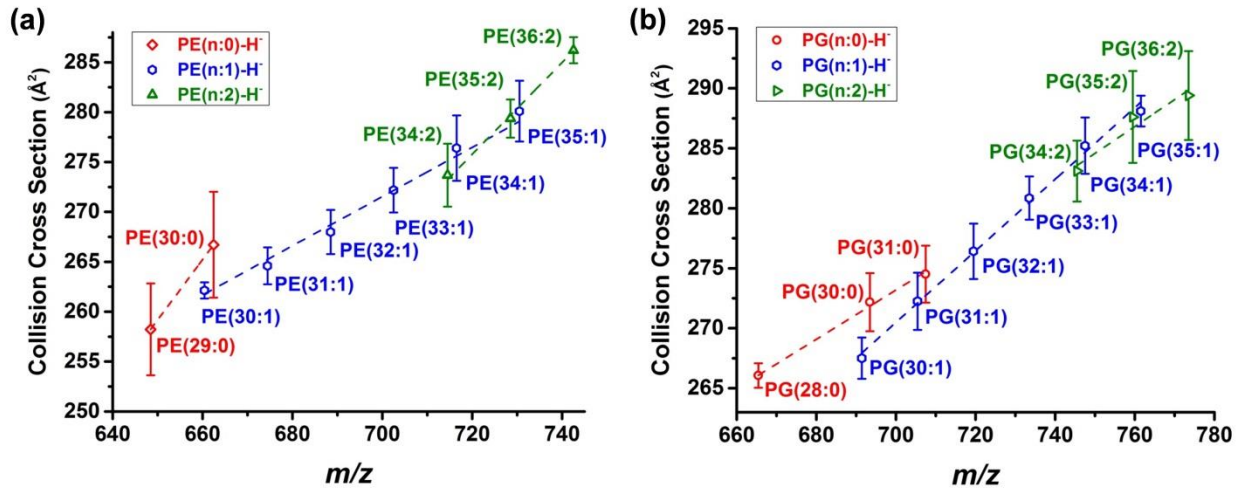

Figure S3. Collision cross sections for lipid subclasses. (a) The CCS values of deprotonated PE(n:0), PE(n:1), and PE(n:2) species as a function of acyl chain lengths show three separate trend lines. (b) The CCS values of deprotonated PG(n:0), PG(n:1), and PG(n:2) also follow linear relationships with the lengths of the acyl chains.

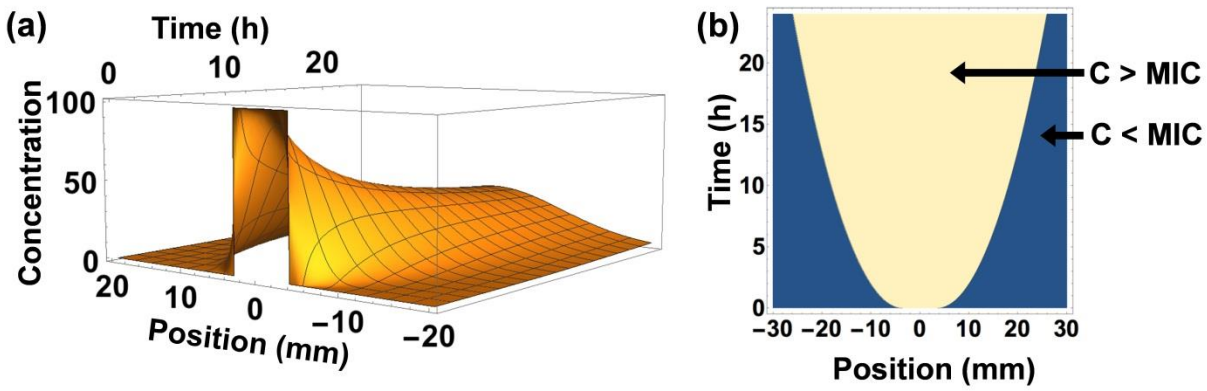

Figure S4. (a) Calculated concentration distribution as a function of position and time, (b) Change in minimum inhibitory concentration (MIC) boundary over 24 h.

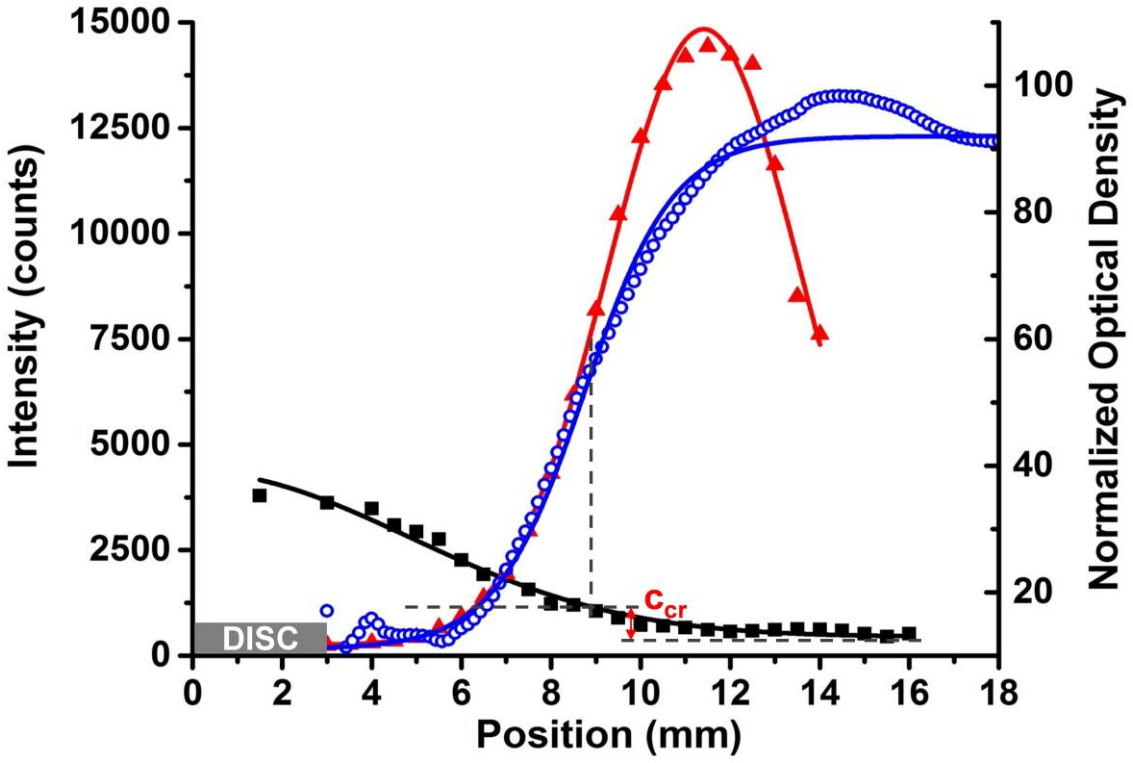

Figure S5. Profiling of streptomycin and PG(34:1) by LAESI-MS in the KB susceptibility test for *E. coli* colonies after 21 h of incubation. The one-dimensional diffusion model (black solid line), $y = i_b + \frac{i_o}{2}\left[\mathrm{erf}\left(\frac{a+x}{2\sqrt{D\times t}}\right) - \mathrm{erf}\left(\frac{-a+x}{2\sqrt{D\times t}}\right)\right]$, was fitted to the measured streptomycin intensities (■), with a = 0.3 cm, and t = 75600 s known parameters. The fitting yielded values for i_b = 446.6, i_0 = 7850.0, and the streptomycin diffusion coefficient, $D = 1.3 \times 10^{-6}$ cm^2/s. A sigmoidal growth curve, and a Gaussian were fitted for the optical density profile (○), and the PG(34:1) ion intensity distribution (▲), respectively. The center of the antibiotic disc was at the origin (x = 0), and the c_{cr} value was determined as the streptomycin concentration at the position with 50% of the microorganisms inhibited.

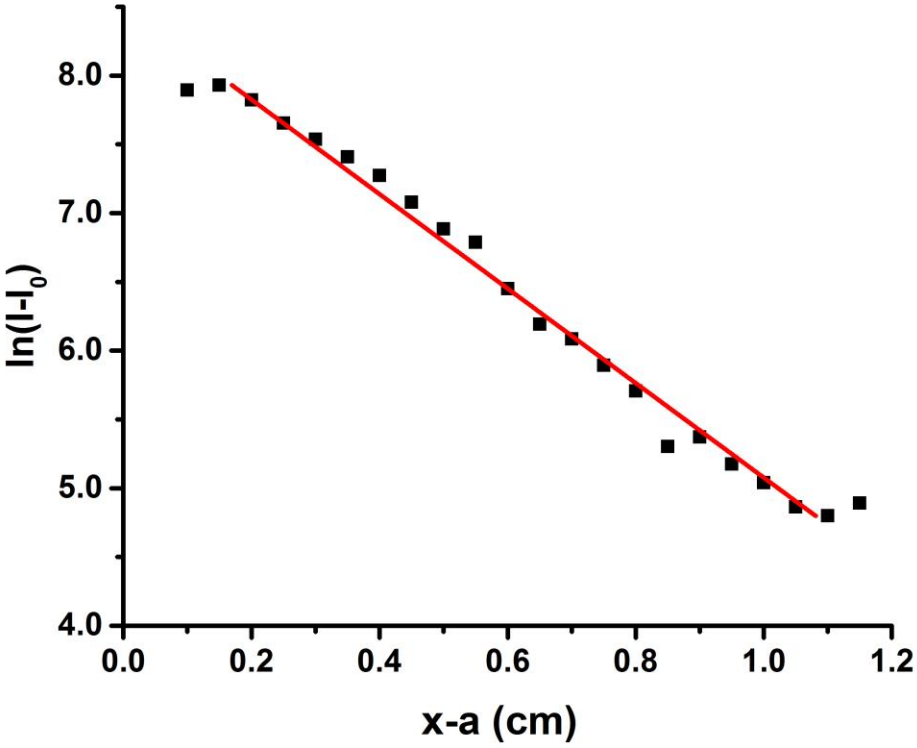

Figure S6. Signal intensity profile within the ZOI transformed according to the Vesterdal antibiotic diffusion model,[5, 6] $\ln(2c) = \ln(c_0) - \frac{x-a}{\sqrt{\pi D t}}$, where c is the antibiotic concentration corresponding to the I-I_0 streptomycin signal intensity, I_0 is the background intensity, c_0 is the initial concentration, a is the radius of the antibiotics disc, t is the diffusion time, and D is the diffusion coefficient. The slope was determined by linear regression (r^2 = 0.98) and a diffusion coefficient of $D = 3.6 \times 10^{-7}$ cm^2/s was recovered.

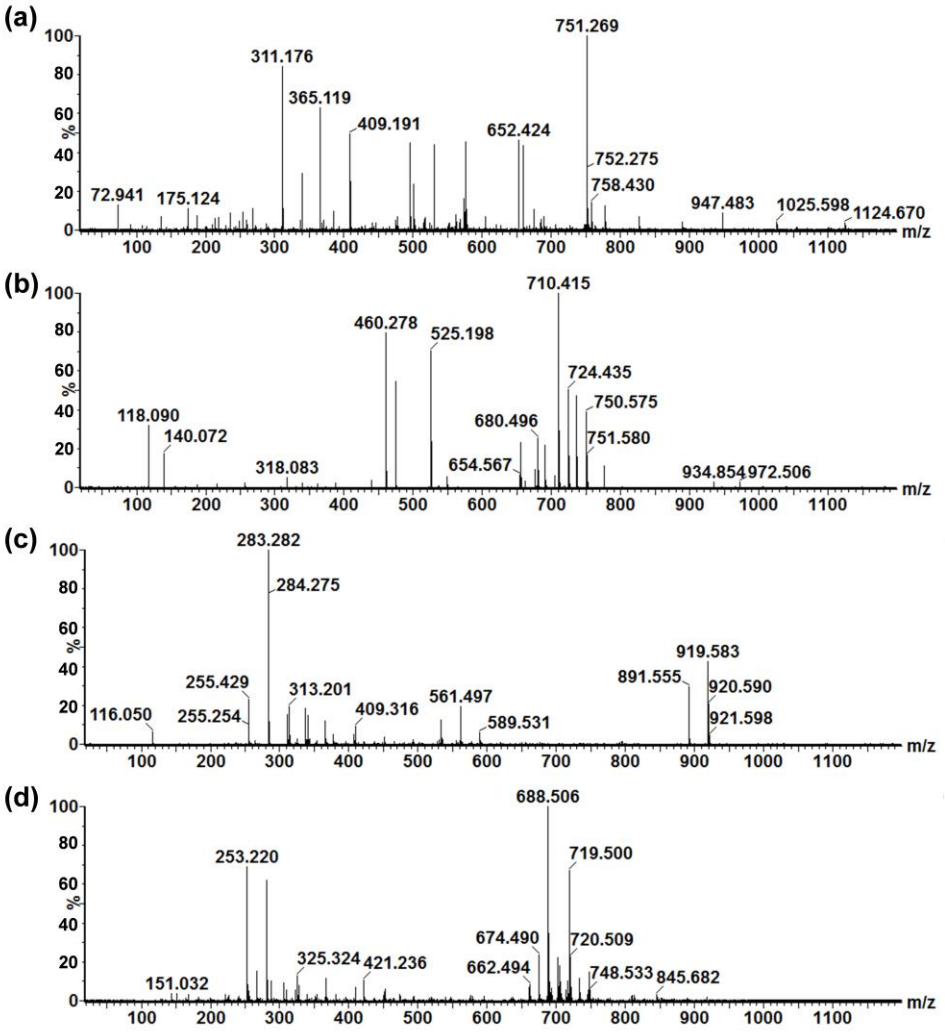

Figure S7. Comparison of LAESI mass spectra in positive ion mode from (a) blank medium and (b) *E. coli* colonies after blank subtraction, and in negative ion mode from (c) blank medium and (d) *E. coli* colonies after blank subtraction.

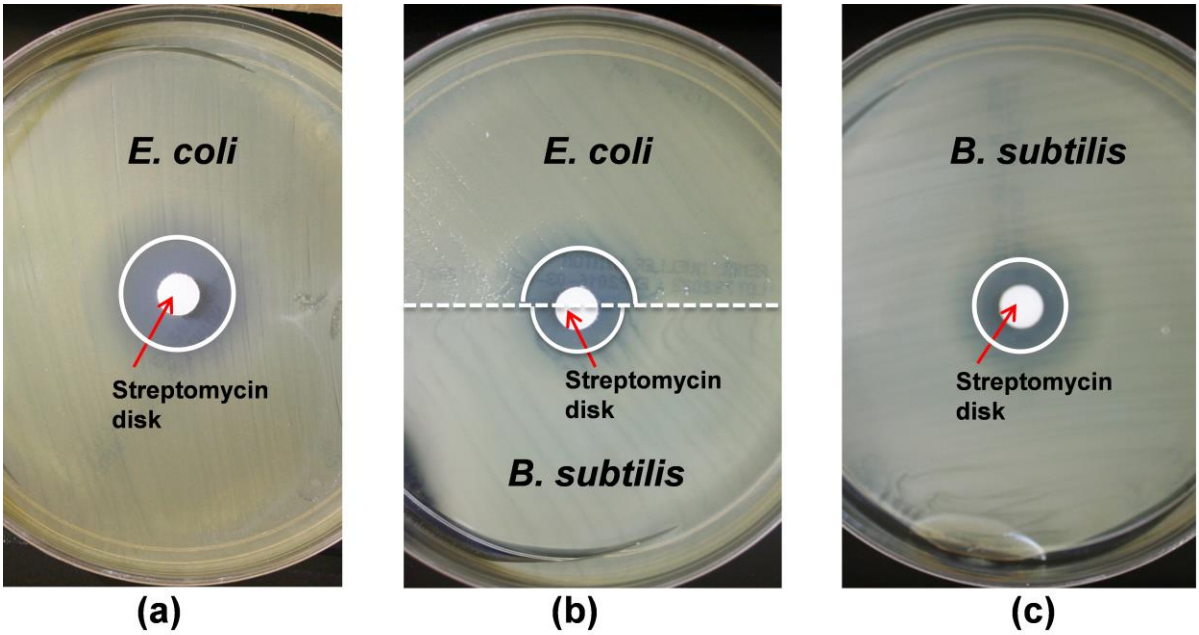

Figure S8. Susceptibility test by KB method performed for (a) *E. coli*, (b) *E.* coli and *B. subtilis* colonies cultured adjacent to each other, and (c) *B. subtilis*.

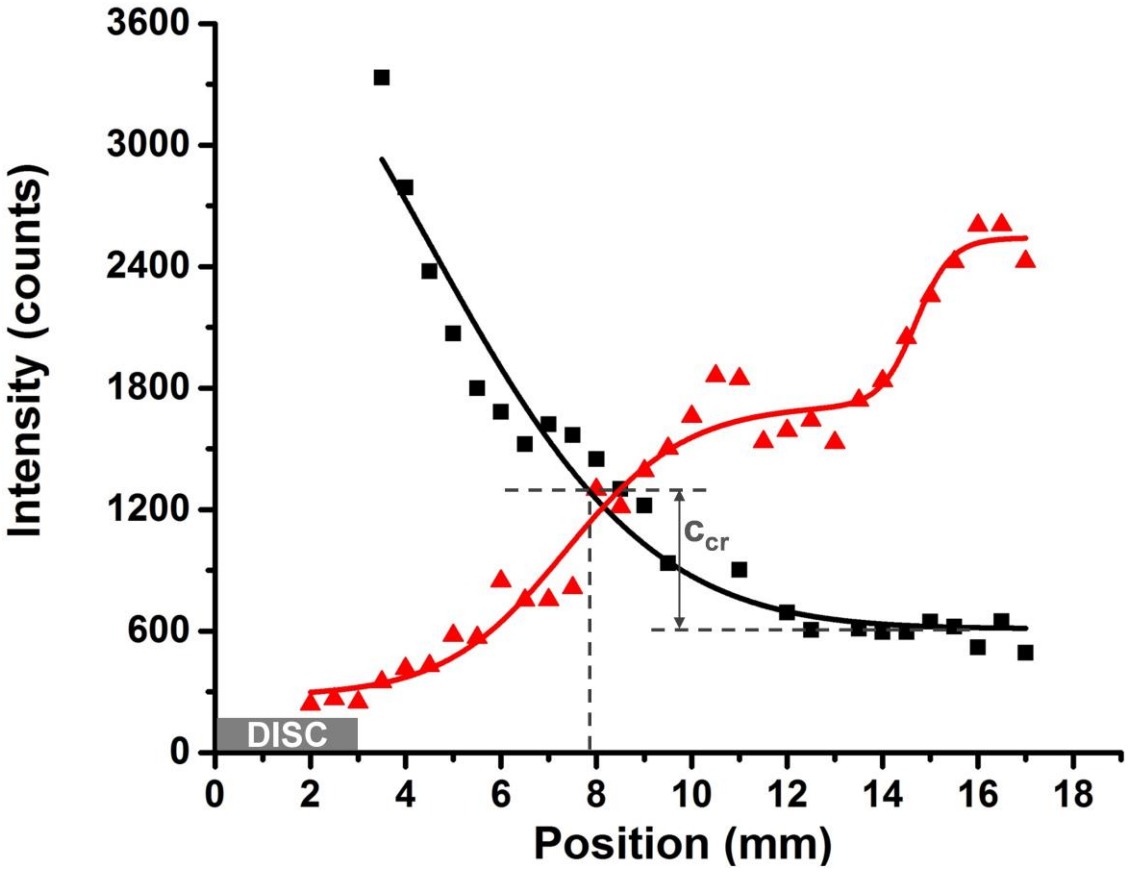

Figure S9. Spatial resolution and sensitivity of LAESI-MS enables susceptibility testing after only 5 h by profiling streptomycin and PE(16:0/16:1) in KB test for *E. coli***.** The one-dimensional diffusion model (black solid line), $y = i_b + \frac{i_0}{2}\left[\mathrm{erf}\left(\frac{a+x}{2\sqrt{D\times t}}\right) - \mathrm{erf}\left(\frac{-a+x}{2\sqrt{D\times t}}\right)\right]$, was fitted to the measured streptomycin intensities (■), with a = 0.3 cm, and t = 18000 s as known parameters. The fitting yielded values for i_b = 612.3, i_0 = 5879.0, and the streptomycin diffusion coefficient, $D = 4.7 \times 10^{-6}$ cm^2/s. A sigmoidal growth curve (Double Boltzmann) was fitted for the PE(16:0/16:1) ion intensity distribution (▲). The center of the antibiotic disc was at the origin (x = 0), and the c_{cr} value was determined as the streptomycin concentration at the position where 50% of the microorganisms were inhibited.

Table S1. Tentative identification of detected metabolites from colonies and cell pellets of *B. subtilis* and *E. coli*. The reference $CCS_{ref.}$ values were obtained from the literature or from our own database.[7]

Metabolite	Formula	$m/z_{calc.}$	*E. coli* $m/z_{meas.}$	Δm (mDa)	*B. subtilis* $m/z_{meas.}$	Δm (mDa)	$CCS_{meas.}$ (Å²)	$CCS_{ref.}$ (Å²)	ΔCCS (%)
Level 1									
acetylspermidine*[a]	$[C_9H_{21}N_3O+H]^+$	188.176	188.176	-0.3	188.177	0.7	136	146	10
glutathione*[a]	$[C_{10}H_{17}N_3O_6S-H]^-$	306.076	306.075	-1.0	306.077	1.0	159	159	0
	$[C_{10}H_{17}N_3O_6S+H]^+$	308.092	308.091	-0.6	308.091	-0.6	159	165	3.8
	$[C_{10}H_{17}N_3O_6S+Na-2H]^-$	328.058	328.057	-0.9	328.058	0.1	160	160	0
ATP*[a]	$[C_{10}H_{16}N_5O_{13}P_3-H]^-$	505.988	505.982	-5.9	505.974	-13.9	185	186	0.5
Level 2									
xanthine*[a]	$[C_5H_4N_4O_2-H]^-$	151.026	151.025	-0.6	151.025	-0.6	119	119	0
AMP*[a]	$[C_{10}H_{14}N_5O_7P-H]^-$	346.055	346.054	-1.3	346.051	-4.3	169	169	0
Level 3									
valine	$[C_5H_{11}NO_2+H]^+$	118.087	118.085	-1.8	118.087	0.2	117	124	6
hypoxanthine[a]	$[C_5H_4N_4O-H]^-$	135.031	135.028	-2.7	135.031	0.3	118	118	0
	$[C_5H_4N_4O+H]^+$	137.046	137.048	1.7	137.046	-0.3	112	120	7.1
valine	$[C_5H_{11}NO_2+Na]^+$	140.069	140.068	-0.7	140.067	-1.7	125		
D-alanyl-D-alanine	$[C_6H_{12}N_2O_3-H]^-$	159.077	159.079	2.0	159.077	0.0	129		
γ-L-glutamyl methylamide	$[C_6H_{12}N_2O_3-H]^-$	159.077	159.079	2.0	159.077	0.0	129		
glycerol monophosphate[a]	$[C_3H_9O_6P-H]^-$	171.006	171.009	3.2	171.006	0.2	127	121	4.7
S-methylmethionine	$[C_6H_{14}NO_2S+Na-2H]^-$	185.049	185.056	7.4	185.056	7.4	137		
ethylthioadenosine	$[C_{12}H_{17}N_5O_3S-H]^-$	310.097	310.101	3.6	310.101	3.6	162		
S-(hydroxymethyl)glutathione	$[C_{11}H_{19}N_3O_7S-H]^-$	336.087	336.093	6.5	336.054	-32.5	162		
dAMP	$[C_{10}H_{14}N_5O_6P+Na-2H]^-$	352.042	352.040	-2.3	352.040	-2.3	161		
xanthylic acid[a]	$[C_{10}H_{13}N_4O_9P-H]^-$	363.034	363.035	0.8	363.033	-1.2	161	162	0.6

S-formylglutathione	$[C_{11}H_{17}N_3O_7S+K]^+$	374.042	374.039	-3.4	374.037	-5.4	164		
dCDP[a]	$[C_9H_{15}N_3O_{10}P_2-H]^-$	386.015	386.016	0.6	386.015	-0.4	173	169	2.3
dGDP*[a]	$[C_{10}H_{15}N_5O_{10}P_2-H]^-$	426.022	426.018	-3.6	426.022	0.4	181	176	2.8
ADP*[a]	$[C_{10}H_{15}N_5O_{10}P_2-H]^-$	426.022	426.018	-3.6	426.022	0.4	181	180	0.6
GDP[a]	$[C_{10}H_{15}N_5O_{11}P_2-H]^-$	442.017	442.017	0.5	442.016	-0.5	178	178	0
retinoyl glucuronide	$[C_{26}H_{36}O_8-H]^-$	475.233	475.234	0.8	475.234	0.8	202		
dTDP-D-glucose	$[C_{16}H_{26}N_2O_{16}P_2-H]^-$	563.068	563.070	2.1	563.070	2.1	200		
dTDP-D-galactose	$[C_{16}H_{26}N_2O_{16}P_2-H]^-$	563.068	563.070	2.1	563.070	2.1	200		
UDP-glucose*[a]	$[C_{15}H_{24}N_2O_{17}P_2-H]^-$	565.047	565.054	6.8	565.046	-1.2	203	204	0.5
UDP-D-galactose*	$[C_{15}H_{24}N_2O_{17}P_2-H]^-$	565.047	565.054	6.8	565.046	-1.2	203		
UDP-N-acetylglucosamine[a]	$[C_{17}H_{27}N_3O_{17}P_2-H]^-$	606.074	606.074	0.3	606.072	-1.7	218	222	0.2
UDP-N-Acetyl-D-mannosamine	$[C_{17}H_{27}N_3O_{17}P_2-H]^-$	606.074	606.074	0.3	606.072	-1.7	218		
surfactin-C14	$[C_{52}H_{91}N_7O_{13}-H]^-$	1020.660			1020.630	-31.6	339		
surfactin-C15	$[C_{53}H_{93}N_7O_{13}-H]^-$	1034.680			1034.680	2.7	342		

*Tandem MS was performed for ion identification.

[a]CCS value was compared with that of a reference standard analyzed under identical experimental conditions.

Table S2. Tentative identification of detected fatty acids and lipids from colonies and cell pellets of *B. subtilis* and *E. coli*. The reference $CCS_{ref.}$ values were obtained from the literature.[8]

Metabolite	Formula	$m/z_{calc.}$	*E. coli* $m/z_{meas.}$	Δm (mDa)	*B. subtilis* $m/z_{meas.}$	Δm (mDa)	$CCS_{meas.}$ (Å²)	$CCS_{ref.}$ (Å²)	ΔCCS (%)
Level 2									
PE(16:0/16:1)*	$[C_{37}H_{72}NO_8P\text{-}H]^-$	688.492	688.492	0.3	688.491	-0.7	268		
	$[C_{37}H_{72}NO_8P+H]^+$	690.507	690.508	0.6	690.507	-0.4	283		
	$[C_{37}H_{72}NO_8P+K]^+$	728.463	728.465	1.8	728.468	4.8	292		
	$[C_{37}H_{72}NO_8P+2Na\text{-}H]^+$	734.471	734.470	-1.2	734.472	0.8	297		
PE(16:0/17:1)*	$[C_{38}H_{74}NO_8P\text{-}H]^-$	702.507	702.507	0.0	702.507	-0.4	272		
	$[C_{38}H_{74}NO_8P+H]^+$	704.523	704.523	0.0	704.523	0.0	289		
	$[C_{38}H_{74}NO_8P+Na]^+$	726.505	726.505	0.1	726.505	0.1	297		
PE(16:0/18:1)*	$[C_{39}H_{76}NO_8P\text{-}H]^-$	716.523	716.521	-2.0	716.522	-1.0	276	272	1.4
	$[C_{39}H_{76}NO_8P+H]^+$	718.539	718.537	-1.7	718.538	-0.7	292		
PG(16:0/16:1)*	$[C_{38}H_{73}O_{10}P\text{-}H]^-$	719.486	719.487	0.7	719.485	-1.3	276		
PG(16:1/17:0)*	$[C_{39}H_{75}O_{10}P\text{-}H]^-$	733.502	733.502	0.0	733.502	0.0	281		
PE(18:1/18:1)*	$[C_{41}H_{78}NO_8P\text{-}H]^-$	742.539	742.536	-2.7	742.538	-0.7	286	279	2.4
	$[C_{41}H_{78}NO_8P+H]^+$	744.554	744.562	7.7	744.550	-0.3	293		
PG(16:0, 18:1)*	$[C_{40}H_{77}O_{10}P\text{-}H]^-$	747.518	747.516	-1.6	747.517	-0.6	285	281	1.4
PG(16:0/19:1)*	$[C_{41}H_{79}O_{10}P\text{-}H]^-$	761.533	761.526	-7.3	761.531	-2.3	288		
Level 3									
FA(18:1)	$[C_{18}H_{34}O_2\text{-}H]^-$	281.248	281.249	1.0	281.250	2.0	178	175	1.7
FA(14:1)	$[C_{14}H_{26}O_2\text{-}H]^-$	225.185	225.188	2.6	225.185	-0.4	160		
FA(16:1)	$[C_{16}H_{30}O_2\text{-}H]^-$	253.217	253.216	-0.7	253.217	0.3	168		
FA(17:1)	$[C_{17}H_{32}O_2\text{-}H]^-$	267.232	267.232	-0.4	267.233	0.6	172		
FA(19:1)	$[C_{19}H_{36}O_2\text{-}H]^-$	295.264	295.260	-3.7	295.264	0.3	183		

FA(20:1)	$[C_{20}H_{38}O_2\text{-}H]^-$	309.279	309.283	3.7	309.279	-0.3	187	183	2.1
LysoPE(16:1)	$[C_{21}H_{42}NO_7P\text{-}H]^-$	450.262	450.262	-0.1	450.261	-1.1	208	210	1
LysoPE(16:0)	$[C_{21}H_{44}NO_7P\text{-}H]^-$	452.278	452.275	-2.7	452.277	-0.7	210	212	1
LysoPE(17:1)	$[C_{22}H_{44}NO_7P\text{-}H]^-$	464.278	464.277	-0.7	464.277	-0.7	211		
PE(29:0)	$[C_{34}H_{68}NO_8P\text{-}H]^-$	648.460	648.458	-2.4	648.459	-1.4	258		
PE(30:1)	$[C_{35}H_{68}NO_8P\text{-}H]^-$	660.460	660.460	-0.4	660.460	-0.4	262		
	$[C_{35}H_{68}NO_8P+H]^+$	662.476	662.480	3.9	662.478	1.9	265		
	$[C_{35}H_{68}NO_8P+Na]^+$	684.458	684.457	-1.0	684.464	6.0	280		
PE(30:0)	$[C_{35}H_{70}NO_8P\text{-}H]^-$	662.476	662.475	-1.1	662.478	1.9	267		
PG(28:0)	$[C_{34}H_{67}O_{10}P\text{-}H]^-$	665.439	665.437	-2.3	665.458	18.7	266		
PE(14:0/17:1)* or PE(16:0/15:1)* or PE(16:1/15:0)*	$[C_{36}H_{70}NO_8P\text{-}H]^-$	674.476	674.476	-0.1	674.475	-1.1	265		
	$[C_{36}H_{70}NO_8P+H]^+$	676.492	676.492	0.3	676.491	-0.7	278		
	$[C_{36}H_{70}NO_8P+Na]^+$	698.474	698.474	0.4			285		
PG(30:1)	$[C_{36}H_{69}O_{10}P\text{-}H]^-$	691.455	691.465	10.0			268		
PG(30:0)	$[C_{36}H_{71}O_{10}P\text{-}H]^-$	693.471	693.471	0.4	693.471	0.4	272		
PE(31:0)	$[C_{36}H_{72}NO_8P+Na]^+$	700.489	700.490	0.7			290		
PG(31:1)	$[C_{37}H_{71}O_{10}P\text{-}H]^-$	705.471	705.472	1.4	705.479	8.4	272		
PG(31:0)	$[C_{37}H_{73}O_{10}P\text{-}H]^-$	707.486	707.485	-1.3	707.484	-2.3	275		
PE(34:2)	$[C_{39}H_{74}NO_8P\text{-}H]^-$	714.507	714.507	-0.4	714.506	-1.4	274	271	1.1
PE(35:2)	$[C_{40}H_{76}NO_8P\text{-}H]^-$	728.523	728.527	4.0	728.524	1.0	279		
PE(35:1)	$[C_{40}H_{78}NO_8P\text{-}H]^-$	730.539	730.533	-5.7	730.537	-1.7	280		
	$[C_{40}H_{78}NO_8P+H]^+$	732.554	732.556	1.7	732.553	-1.3	298		
PE(34:1)	$[C_{39}H_{76}NO_8P+Na]^+$	740.521	740.521	0.4	740.519	-1.6	298		
PE(33:1)	$[C_{38}H_{74}NO_8P+K]^+$	742.479	742.491	12.1	742.481	2.1	303		
PG(34:2)	$[C_{40}H_{75}O_{10}P\text{-}H]^-$	745.502	745.503	1.0	745.501	-1.0	283	279	1.4
PG(34:1)	$[C_{40}H_{77}O_{10}P+H]^+$	749.533	749.549	15.8	749.547	13.8	290		
PS(O-34:0)	$[C_{40}H_{80}NO_9P+H]^+$	750.565	750.558	-6.9			305		

PG(34:0)	$[C_{40}H_{79}O_{10}P+H]^+$	751.549	751.559	10.1	751.552	3.1	308		
PG(35:2)	$[C_{41}H_{77}O_{10}P-H]^-$	759.518	759.519	1.4	759.517	-0.6	288		
PG(36:2)	$[C_{42}H_{79}O_{10}P-H]^-$	773.533	773.531	-2.3	773.532	-1.3	289	289	0
PG(O-42:1)	$[C_{48}H_{95}O_9P-H]-$	845.664	845.663	-0.5	845.658	-5.5	315		
PS(37:4)	$[C_{43}H_{76}NO_{10}P-H]-$	796.513			796.509	-3.8	295		

*Tandem MS was performed on the cell pellets for ion identification.

Abbreviations: FA - fatty acids, PE - phosphatidylethanolamine, PG - phosphatidylglycerol, and PS - phosphatidylserine.

[1] H. Li, B. K. Smith, L. Márk, P. Nemes, J. Nazarian, A. Vertes, *Int. J. Mass spectrom.* **2015**, *377*, 681-689.

[2] L. W. Sumner, A. Amberg, D. Barrett, M. H. Beale, R. Beger, C. A. Daykin, T. W. M. Fan, O. Fiehn, R. Goodacre, J. L. Griffin, T. Hankemeier, N. Hardy, J. Harnly, R. Higashi, J. Kopka, A. N. Lane, J. C. Lindon, P. Marriott, A. W. Nicholls, M. D. Reily, J. J. Thaden, M. R. Viant, *Metabolomics* **2007**, *3*, 211-221.

[3] J. Schindelin, I. Arganda-Carreras, E. Frise, V. Kaynig, M. Longair, T. Pietzsch, S. Preibisch, C. Rueden, S. Saalfeld, B. Schmid, J.-Y. Tinevez, D. J. White, V. Hartenstein, K. Eliceiri, P. Tomancak, A. Cardona, *Nat Meth* **2012**, *9*, 676-682.

[4] B. S. Bokstein, D. J. Srolovitz, M. I. Mendelev, *Thermodynamics and kinetics in materials science*, Oxford University Press, **2005**.

[5] D. A. Mitchison, C. C. Spicer, *J. Gen. Microbiol.* **1949**, *3*, 184-203.

[6] J. W. Mellor, *Higher Mathematics for Students of Chemistry and Physics*, London, Longmans, Green and co., **1902**.

[7] G. Paglia, J. P. Williams, L. Menikarachchi, J. W. Thompson, R. Tyldesley-Worster, S. Halldorsson, O. Rolfsson, A. Moseley, D. Grant, J. Langridge, B. O. Palsson, G. Astarita, *Anal. Chem.* **2014**, *86*, 3985-3993.

[8] G. Paglia, P. Angel, J. P. Williams, K. Richardson, H. J. Olivos, J. W. Thompson, L. Menikarachchi, S. Lai, C. Walsh, A. Moseley, R. S. Plumb, D. F. Grant, B. O. Palsson, J. Langridge, S. Geromanos, G. Astarite, *Anal. Chem.* **2015**, *87*, 1137-1144.